

# A Precise Point Positioning Filtering Method for Navigation and Orbit Determination of Low Earth Orbiters

Takahiro YOSHIOKA\*\* and Masaaki MURATA\*

A new precise point positioning (PPP) technique for on-orbit navigation (NAV) and precision orbit determination (POD) of LEO satellites is proposed. A dual-frequency PPP filter is developed by assuming simple white noise processes for both position deviation (from the pre-determined reference orbit) and receiver clock. The filter performance is assessed by processing one-day GPS data collected with a dual-frequency receiver onboard the LEO satellite CHAMP. The results show that dual-frequency PPP in space is capable of producing NAV solution with 3D positional accuracy of about one meter, and POD solution of about 0.6 meters, both in 95 percentile.

**Key Words:** PPP, GPS, satellite navigation, EKF, UKF, CHAMP

## 1. Introduction

A new technique called Precise Point Positioning (PPP) has been attracting precision geo-science and navigation community, as it would have a potential of providing highly accurate point positioning with only a single GPS receiver. The PPP accuracy, which is almost comparable to that of kinematic GPS (KGPS), has been reported for terrestrial and aerial navigation users<sup>1)-3)</sup>. Such a PPP technique became possible with the availability of precise orbits and clock correction information for the GPS satellites, which the International GNSS Service (IGS) has begun generating and disseminating since 1994 as an international civil cooperation. Compared to DGPS techniques<sup>4)</sup>, PPP has the obvious advantages of simplified system design, operational flexibility (i.e., no specific operational restrictions), and cost reduction. PPP could therefore be a vital alternative to the conventional carrier phase DGPS.

For space PPP, a number of studies on LEO precision orbit determination (POD) in post-mission mode have been carried out<sup>5)-8)</sup>, but very few studies have focused on real-time on-orbit navigation application (NAV) for LEO satellites. In this paper we propose a simple and efficient approach to LEO NAV as well as LEO POD, which relies solely on raw un-differenced pseudorange and carrier phase data. Therefore it differs from the previous investigations (primarily dedicated to LEO POD) in the algorithm: for example, Bock et al.<sup>6)</sup> used un-differenced pseudorange and

epoch-by-epoch carrier phase difference data, and also Bisnath et al.<sup>7)</sup> used double-differenced pseudorange and triple-differenced carrier phase data.

In 2006 and 2007, we developed a basic PPP software at National Defense Academy (NDA) for terrestrial and aerial vehicular navigation applications and assessed its performance indicating the horizontal accuracy at a few centimeters for static antennas and at better than a few decimeters for moving antennas<sup>9)-10)</sup>. This PPP software was intensively modified for space navigation users and evaluated by applying to the 24-hour dataset collected on CHAMP, German LEO satellite. This paper gives design philosophy of a dual-frequency PPP filter and analysis results of positioning performance for both NAV and POD.

## 2. PPP Filter Design

Implicitly assumed is that the onboard receiver is dual-frequency so that ionospheric-free pseudorange and carrier phase data are constructed. In that case the observation equations are described in the form of the linear combinations for each satellite:

$$P = \frac{f_1^2 P_1 - f_2^2 P_2}{f_1^2 - f_2^2} \quad (1)$$

$$= \rho + c(dt + \delta^r) - c(dt_{SV} + \delta_{SV}^r) + \varepsilon_{PR}$$

$$C = \frac{f_1^2 C_1 - f_2^2 C_2}{f_1^2 - f_2^2} \quad (2)$$

$$= \rho + c(dt + \delta^r) - c(dt_{SV} + \delta_{SV}^r) + \tilde{N} + \varepsilon_{CP}$$

$$\tilde{N} = \frac{cf_1 N_1 - cf_2 N_2}{f_1^2 - f_2^2} \quad (3)$$

\* Professor and Corresponding Author, Aerospace Engineering, National Defense Academy, Yokosuka, Kanagawa (E mail to: murata@gnss.co.jp)

\*\* Graduate Student, Aerospace Engineering, National Defense Academy, Yokosuka, Kanagawa

(Received October 12, 2010)

where  $P_i$  is the measured pseudorange on carrier wave  $L_i$  ( $i=1,2$ );  $C_i$  is the measured carrier phase on  $L_i$ ;  $\rho$  is the true geometric range;  $c$  is the speed of light;  $dt$  is the receiver clock bias;  $\delta^r$  is the relativistic effect on receiver clock;  $dt_{SV}$  is the transmitter clock bias;  $\delta_{SV}^r$  is the relativistic effect on transmitter clock;  $f_i$  is the frequency of  $L_i$ ;  $N_i$  is the integer phase ambiguity on  $L_i$ ;  $\tilde{N}$  is the floating ambiguity; and  $\varepsilon_i$  represents the residual measurement error including random noise. The measurement error is assumed to be normally distributed with mean zero and elevation-dependent standard deviation (SD) of

$$\sigma_k(el) = \frac{\sigma_{0,k}}{\sin \sqrt{el^2 + a_k^2}}, k = P, C \quad (4)$$

where  $\sigma_{0,k}$  is a nominal SD along the zenith direction,  $el$  is the elevation angle above local horizon, and  $a_k$  is a tuning parameter of constant (set zero throughout this study). Navigation users can use the precise orbits and clocks produced by IGS. Currently the IGS's official products for precise orbits and clocks are in three categories: UltraRapid, Rapid, and Final. Among these products, only the UltraRapid orbit and clock can be used in real-time. In this paper, however, we used the Final product of the 15-minute precise orbits and 30-second clock corrections, which were computed at the CODE (Center for Orbit Determination in Europe), one of the IGS analysis centers. When necessary they were interpolated using Lagrange's polynomial, that is, the 9th order polynomial for orbits and the 2nd order polynomial for clock corrections. Also, the correction for the center-of-mass offset to the transmitting antenna was applied (**Fig.1**).

The unknown parameters in the PPP filter nominally consist of the position components ( $\vec{r}$ ) of the receiver antenna, a receiver clock bias ( $b$ ), and ionospheric-free (non-integer) ambiguities ( $\tilde{N}$ , max.12) of the un-differenced carrier phase data. *The position components ( $\vec{r}$ ) are the positional deviation from a pre-determined reference trajectory of the LEO satellite.* The float ambiguities are modeled as a piece-wise constant corrupted with white noises. All unknowns except for the float ambiguities are modeled as Gaussian white noise processes with mean zero and specified variances. The clock model like this is often called a white noise clock. The white noise models are the simplest mathematically and so with less demanding for computation. Note that there is no rationale

for Gaussianity with zero mean, and that it is only an assumption made for technical convenience. The other models, such as random walk, first-order Markov model, etc., could of course be used but the improvement in positional performance will be marginal.

The state equations are thus described in a simple linear discrete form as follows:

$$\vec{r}_{j+1} = \vec{w}_{r,j}, \vec{w}_{r,j} \sim N(0, q_r I_{3 \times 3}) \quad (5)$$

$$b_{j+1} = w_{b,j}, w_{b,j} \sim N(0, q_b) \quad (6)$$

$$\tilde{N}_{j+1} = \tilde{N}_j + \vec{w}_{\tilde{N},j}, \vec{w}_{\tilde{N},j} \sim N(0, q_{\tilde{N}} I_{12 \times 12}) \quad (7)$$

where  $I_{n \times n}$  denotes an  $n \times n$  unit matrix. The magnitude of covariance matrices  $q_r, q_b$  and  $q_{\tilde{N}}$  for the white noises

$\vec{w}_r, w_b$  and  $\vec{w}_{\tilde{N}}$  is tuning parameters. Hereafter,

$\vec{x} \sim N(\vec{m}, P)$  means that  $\vec{x}$  is normally distributed with mean  $\vec{m}$  and covariance matrix  $P$ . As the means of constructing the PPP filter, we chose the conventional Extended Kalman Filter (EKF)<sup>(11)~(12)</sup> and the Unscented Kalman Filter (UKF)<sup>(13)</sup>, an alternative to the EKF.

### 3. Analysis Results

#### 3.1 LEO Data

The CHAMP (CHALLENGING Mini-satellite Payload for geophysical research and application) is a German LEO satellite designed for geo-science and atmospheric research and managed by the GeoForschungs Zentrum (GFZ). Its main scientific mission goals are to provide highly precise gravity field, magnetic field, radio occultation measurements, and GPS altimetry over a 5-year period. Fig.1 shows the satellite configuration with the location of the GPS receiver antennae for POD (and NAV). One-day dataset collected on November 18, 2006, were focused in the present paper. The data included dual-frequency pseudorange and carrier phase taken by a "BlackJack" 12-channel receiver. They were unedited with the sampling interval of 10 seconds. While the cataloged values of raw, un-differenced data precision are 10-20 cm in pseudorange and 0.05 cm in carrier phase, we assigned the values of 50 cm and 1 cm, respectively, as the nominal observation error standard deviation (see Eq.(4)) for the ionosphere-free combination in the zenith direction, by taking into account

the effect of the remaining residual errors. It should be noted that no attitude information was available for this research. At that time the CHAMP orbited at an altitude of 350 km, with a period of about 90 minutes, an eccentricity of smaller than 0.001, and an inclination of 89 degrees. The corresponding satellite visibility is plotted in Fig.2. The upper (thick) skyline shows the maximum number of GPS satellites all-in-view from CHAMP's receiver, indicating that approximately 8.2 satellites on average were observed at an epoch. The lower (thin) line shows the number of GPS

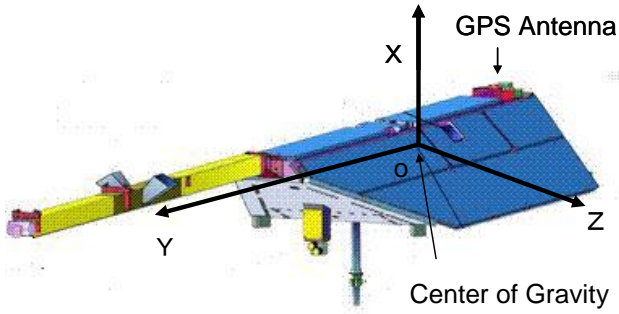


Fig. 1 CHAMP configuration (GFZ Web)

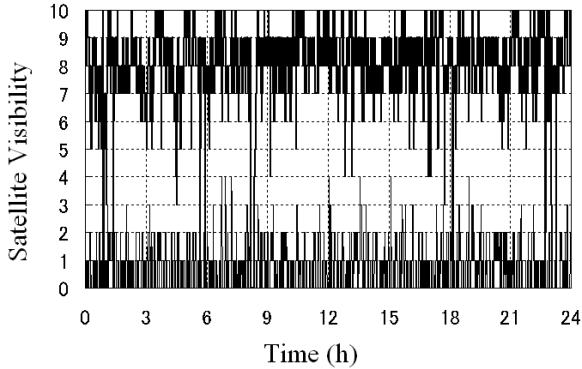


Fig.2 Satellite visibility

satellites with the elevation angle of less than 10 degrees, approximately 0.7 satellites on average.

### 3.2 Reference Orbit Generation

Satellite missions for LEO require real-time or post-flight orbit determination (OD). As usual, post-flight OD is performed by the use of large-scale orbit determination program. On the other hand, the proposed PPP filter is executed assuming a reference orbit with moderate accuracy. For the case that any reference orbit is not available in advance, we have proposed<sup>14)</sup> to generate it using a classical least-squares in which the observation data are an epoch-to-epoch sequence of the *single point positioning solution*, i.e. the 3D position coordinates in the

conventional terrestrial system (CTS) or equivalently in the Earth-centered, Earth-fixed frame (ECEF). Here the coordinate solution is derived by using the pseudorange data only. We call this set of the temporal coordinate solution as the *pseudo-observations*. Satellite dynamics for the batch filter is expressed in the J2000 inertial system as

$$\ddot{\vec{R}} = -\mu \frac{\vec{R}}{R^3} + \vec{f}(t, \vec{R}, \dot{\vec{R}}, \vec{p}) \quad (8)$$

where  $t$  is the Terrestrial Time (TT),  $\mu$  is the gravitational parameter of the Earth,  $\vec{p}$  is the unknown constant parameter vector to be estimated, and  $\vec{f}$  denotes the perturbation acceleration vector. For the Earth gravity computation the NASA's Earth Gravitational Model 1996 (EGM96), truncated up to degree and order 36, was adopted in this research. For the atmospheric density, we can use either exponentially decaying model or the Jacchia-Roberts 1971 model with tabular data consisting of  $F_{10.7}$  solar flux and 3-hourly planetary geomagnetic index  $K_p$ . The Earth orientation parameters (EOP) are required as well. The other forces acting on the satellites, such as solid Earth tide, ocean tide, and earth radiation pressure and relativistic effects, are marginal for a relatively short arc of LEO satellites and hence are not taken into account.

The observation equation is thus described as

$$\vec{r}_{k,obs} = \vec{r}_{k,true} + \vec{\varepsilon}_k \quad (9)$$

where  $\vec{\varepsilon}_k \sim N(0, R_k)$  ( $k = 1, 2, \dots$ ). The single point positioning solution vector  $\vec{r}_{k,obs}$  is calculated in the ECEF frame. The  $3 \times 3$  positioning error covariance matrix  $R_k$  varies with satellite geometry, but we assume they are a diagonal  $\sigma_p^2 I_{3 \times 3}$  where  $\sigma_p = 1$  m is adopted.

In summary, a reference orbit can be calculated by applying the following two-step procedures: first, 1) single point positioning solution (3D coordinates) at each epoch is obtained by the conventional least-squares in which precise orbits and clock corrections are used; and secondly, 2) the orbit is dynamically fitted to the 3D coordinates used as the pseudo-observations.

The above OD scenario was evaluated with varying dynamic models based on the 24-hour CHAMP data, and the resulting orbit accuracy was investigated by the direct difference from the GFZ precise ephemeris. As an example,

**Fig.3** shows the time history of the orbit difference between the generated reference orbit (no drag included) and the truth (i.e. GFZ's precise orbit). The orbit difference from the truth is expressed in the local radial-transverse-normal (RTN) frame (see Appendix A). The error in the transverse direction is the biggest, being the maximum error of about 600 m towards the initial and final epochs. Obviously, this is due to the lack of atmospheric drag force model in the OD process. This orbit was used in this research as the reference orbit for the PPP filter.

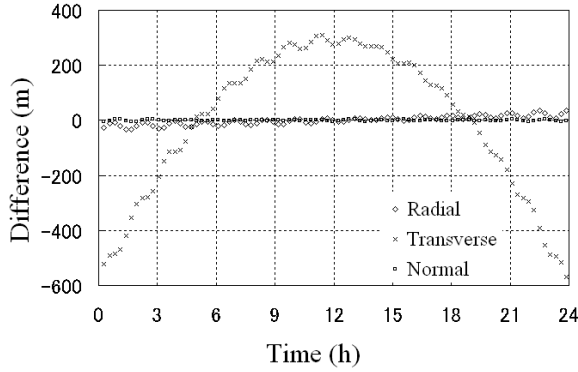


Fig.3 Position difference between the reference orbit and GFZ precise orbit

### 3.3 PPP Results

The 24 hours of observation data were processed by the EKF and the UKF, assuming a nominal model setup and with the mask angle of 10 degrees. The time update portion of the EKF takes the form as follows:

$$\bar{\mathbf{x}}_{j+1} = \phi_j \hat{\mathbf{x}}_j \quad (10)$$

$$\bar{\mathbf{P}}_{j+1} = \phi_j \hat{\mathbf{P}}_j \phi_j^T + \mathbf{Q} \quad (11)$$

where  $\bar{\mathbf{x}} = (\bar{\mathbf{r}}^T \quad b \quad \bar{\mathbf{N}}^T)^T$  is 16-dimensional and

$$\mathbf{Q} = \begin{pmatrix} q_r \mathbf{I}_{3 \times 3} & 0 & 0 \\ 0 & q_b & 0 \\ 0 & 0 & q_{\tilde{\mathbf{N}}} \mathbf{I}_{12 \times 12} \end{pmatrix} \quad (12)$$

In Eqs. (10) and (11) (and also in Appendix B), the upper bar and hat denote the a priori and a posteriori estimate respectively, and the transition matrix  $\phi_j$  is the identity matrix, except for the position and clock bias portions that are zero for the above baseline white noise model. The process noise intensity matrix  $\mathbf{Q}$  can be set up either

empirically or through intensive parameter tuning on the basis of running simulation program of the PPP filter. The selected values are

$$q_r = q_b = 10^6 \text{ m}^2/\text{s} \text{ and } q_{\tilde{\mathbf{N}}} = 10^{-10} \text{ m}^2/\text{s} \text{ for } \mathbf{Q}, \text{ and}$$

$\alpha = 1, \beta = 2, \kappa = 3 - L$  for UKF, where L denotes the dimension of the filter state (see Appendix B for details).

The kinematic CHAMP orbit solution is very sensitive to data editing schemes applied, and therefore online data screening is a prerequisite for the NAV and POD filters. The editing strategies implemented in this paper are shown in **Table 1**. The Melbourne-Wuebbenna (M-W) linear combination is defined as wide-lane carrier phase minus narrow-lane pseudorange, i.e.

$$\begin{aligned} \tilde{\phi} &= \frac{1}{f_1 - f_2} (f_1 \phi_1 - f_2 \phi_2) - \frac{1}{f_1 + f_2} (f_1 P_1 + f_2 P_2) \\ &= \frac{c}{f_1 - f_2} (N_1 - N_2) \end{aligned} \quad (13)$$

and this eliminates the effect of the ionosphere, the geometry, the clocks and the troposphere. Thus, this combination can be used to detect cycle slips in the undifferenced carrier phase data. These editing strategies are able to screen the data in the observation domain, with no need of post-fit residual analysis. Strictly speaking, models for precise orbits and precise clocks have to be consistent

Table 1 Edit criteria for NAV and POD pre-processing

Criterion	Content
Satellite status*	Satellite health, and SV accuracy (from navigation message)**
Cutoff angle*	Reject data with elevation angle less than 10°
Radio signal strength*	Reject data with SNR < 6 (RINEX standard)
Erroneous Pseudorange*	Reject unless $PR_{\min} < PR < PR_{\max}$
Residuals*	Reject if the moving average of the residuals weighted with the reciprocal of the estimation error covariance is larger than the specified level.
Cycle slip*	Reset the filter if the time difference of Melbourne-Wuebbenna linear combination is larger than the specified tolerance.
Isolated epoch of data	Removed by hand (only for POD data).

\* Applied for both NAV and POD data.

\*\* PRN15, decommissioned on 17 Nov. 2006

each other, and it was satisfied in this paper by the use of 15-minute orbits and 30-second clocks both computed by the CODE. Positioning errors between the EKF navigation solution and the truth, i.e. precise dynamic orbit of the GeoForschungsZentrum (GFZ), both expressed in the local radial-transverse-normal (RTN) frame, were computed in which the center-of-mass offset correction against receiver's phase center was applied by assuming that the spacecraft attitude is nominally aligned along the RTN directions.

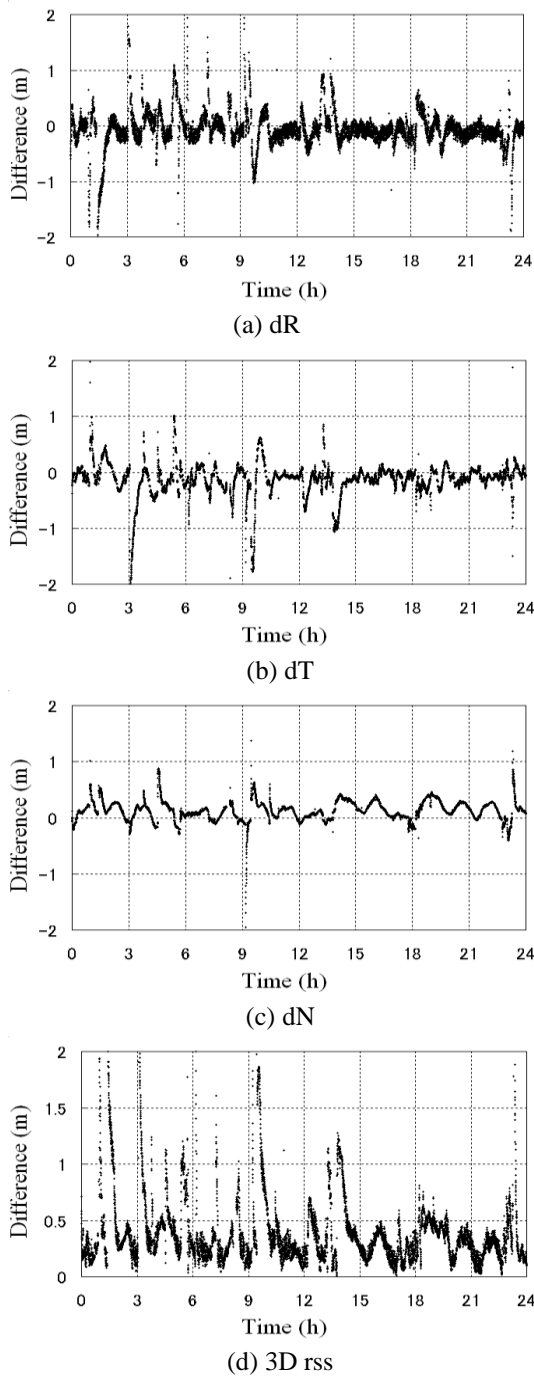


Fig. 4 NAV-EKF positioning errors

Table 2 Positional error of NAV-EKF (Unit:m)

parameter	dR	DT	dN	3D rss
median	0.15	0.13	0.14	0.31
95%	0.87	0.73	0.40	1.13

Table 3 Positional error of NAV-UKF (Unit:m)

parameter	dR	DT	dN	3D rss
median	0.15	0.12	0.14	0.30
95%	0.75	0.76	0.38	1.07

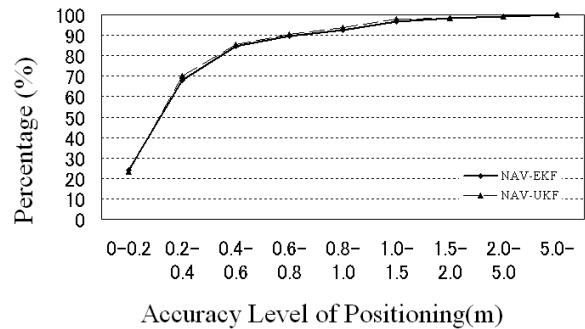


Fig. 5 Histogram of 3D rss positioning errors

For the purpose of saving paper space, only the plots of the NAV-EKF results are shown in **Fig.4**. Fig.4 (a)-(c) plot the positioning errors, i.e. dR, dT, and dN at each of the RTN directions, and Fig.4 (d) shows the 3-dimensional root-sum-squares (3D rss). At first it should be noticed that, opposite to very slow convergence found for the terrestrial or aerial PPP navigation<sup>9)-10)</sup>, the space PPP filter is converging much faster, within several number of observation epochs. This is most likely due to satellite's orbital motion causing rapid change in the measurement geometry. Second, there are many spikes in all plots, some exceeding hundred meters, and they are mostly due to the frequent filter re-initialization when a new satellite is coming up or a cycle slip occurs. In particular, the procedure when a cycleslip has occurred goes as follows: calculate first the prediction of the new ambiguity (with use of the M-W linear combination); and replace the corresponding filter state component with the predicted value and at the same time initialize the corresponding component of the covariance matrix; and then incorporate that carrier phase data into the filter.

Third, the POD result does not change so much from the NAV one, but with rather less spikes because of additional hand editing of separated data and short passes. **Fig.5** shows the histogram of positioning errors for NAV case. **Table 2** and **3** tabulate the median and the 95-percentile point of positional errors in each direction. For NAV solution, positioning accuracy of less than one meter in both radial and transverse components and of less than one-

half meters in the normal component, with 3D accuracy of about one meter, can be achieved (all in the sense of 95 percentile). The NAV solution is not biased so much, at the level of smaller than a decimeter. For POD, positioning accuracy of about one-half meters in all components, with 3D accuracy of about 0.6 meters, can be achieved (in 95 percentile). As seen from Table 3, the UKF provides slightly better positioning results than the EKF, but by paying the extra computational cost. Indeed, it is well recognized that the UKF in its standard form takes much more computational burden than the conventional EKF.

**Fig.6**, a microscopic view of Fig.4 focused over the short period (18 min.) of high quality estimation, shows that the position errors in each direction are more or less oscillating in a saw-shape manner with a period of about 150 s and with a peak-to-peak range of 20 cm for dR, some cm for dT and dN. The oscillatory variation in the radial direction suggests pitching motion around the center of mass of the spacecraft, although the cause of 150 s periodicity is not identified. The result evidences superior accuracy of the PPP filters. **Fig.7** compares convergence property of two filters before and after reset over a period of data gap. Before reset, both filters are in a steady-state with almost equal position errors. Immediately after reset, position errors increase abruptly but decrease gradually as measurements are processed. Clearly, the UKF is more

accurate and faster in convergence than the EKF. This is because of the second order accuracy of the UKF unconditionally.

#### 4. Conclusions

A design methodology of a PPP filter for LEO navigation and orbit determination is proposed and its performance is evaluated in post-mission mode using 24 hours of GPS tracking data collected onboard CHAMP. The potentiality and effectiveness of the PPP filtering approach are demonstrated: the 3D rss positioning accuracy (95 percentile) of about one meter for NAV and of about 0.6 meters for POD can be achieved. The filter generally shows fast convergence due primarily to rapid change of the geometry. However, data editing scheme applied online for NAV or offline for POD extremely affects the positioning performance and should be paid special efforts in its implementation.

#### Acknowledgements

We thank GeoForschungsZentrum (GFZ), Germany, for our access to the CHAMP data, the precise science orbit, and the additional information at the CHAMP Information System and Data Center (ISDC). In particular, the second author is grateful to Dr.C.Reigber and Dr.G.Gendt of GFZ for their cooperation with informative discussions.

#### References

- 1) Y.Gao and K.Chen: Performance Analysis of Precise Point Positioning Using Real-Time Orbit and Clock Products, *Journal of GPS*, **Vol.3**, No.1-2, 95/100 (2004)
- 2) J.Kouba and P.Heroux: Precise Point Positioning Using IGS Orbit and Clock Products, *GPS Solutions*, **Vol.5**, No.2, 12/28 (2001)
- 3) O.L.Colombo et al.: Evaluation of Precise, Kinematic GPS Point Positioning, Proc.of ION GNSS-2004 Meeting, Long Beach, California (2004)
- 4) B.Hofmann-Wellenhof, H.Lichtenegger, and J.Collins: *GPS-Theory and Practice*, 5<sup>th</sup> revised edition, Springer-Verlag (2001)
- 5) S.B.Bisnath and R.B.Langley: Precise A Posteriori Geometric Tracking of Low Earth Orbiters with GPS, *Canadian Aeronautics and Space Journal*, **Vol.45**, No.3, 245/252 (1999)
- 6) H.Bock, et al.: Efficient Precise Orbit Determination of LEO Satellites Using GPS, *Adv.Space Res.*, **Vol.30**, No.2, 295/300 (2002)

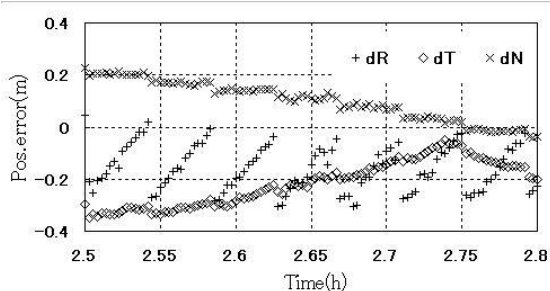


Fig.6 Microscopic view of positional errors

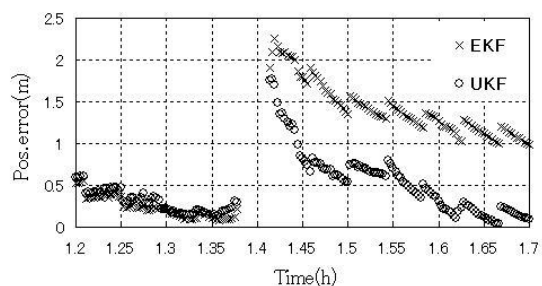


Fig.7 Convergence feature before and after reset

- 7) S.Bisnath: Precise Orbit Determination of Low Earth Orbiters with a Single GPS Receiver-Based, Geometric Strategy, Technical Report No.220, UNB (2004)
- 8) O.L.Colombo and S.B.Luthcke: Kinematic Point Positioning of a LEO with Simultaneous Reduced-Dynamic Orbit Estimation, Proc.of the ION GNSS-2004 Meeting, Long Beach, California (2004)
- 9) M.Honda, M.Murata, and Y.Mizukura: Development and Assessment of GPS Precise Point Positioning Software for Land Vehicular Navigation, SICE e-Journal, **Vol.6**, No.10, 78/84 (2007)
- 10) Y.Shimizu and M.Murata: Flight Evaluation of GPS Precise Point Positioning Software for Helicopter Navigation, SICE JCMSI, **Vol.1**, No.5, 362/367 (2008)
- 11) A.H.Jazwinski: Stochastic Process and Filtering Theory, Academic Press, New York (1970)
- 12) B.D.Tapley, B.E.Schutz, and G.H.Born: Statistical Orbit Determination, Elsevier Academic Press (2004)
- 13) E.A.Wan and R.M. van der: The Unscented Kalman Filter, in *Kalman Filtering and Neural Networks* (edited by S.Haykin), John Wiley & Sons (2001)
- 14) T.Yoshioka: Study on GPS Precise Point Positioning for Navigation and Orbit Determination of LEO Satellite, Master Thesis, National Defense Academy (2010) (in Japanese)

### Appendix A: RTN Frame

Given the position and velocity vectors  $\vec{R}$  and  $\vec{V}$  of the satellite at an epoch in a reference Cartesian coordinate system, we can compute the orthogonal unit vectors as follows:

$$\hat{R} = \frac{\vec{R}}{|\vec{R}|}, \quad \hat{N} = \frac{\vec{R} \times \vec{V}}{|\vec{R} \times \vec{V}|}, \quad \hat{T} = \hat{N} \times \hat{R} \quad (\text{A1})$$

Here,  $\hat{R}$ ,  $\hat{T}$  and  $\hat{N}$  are aligned with the radial, transverse (along-track), and normal (cross-track) directions, respectively. This set of three triads defines the right-handed rotating coordinate system called the radial-transverse-normal (RTN) frame (**Fig.8**). The coordinate transformation matrix from the reference frame to the RTN frame is given by

$$C_{REF}^{RTN} = \begin{pmatrix} \hat{R} & \hat{T} & \hat{N} \end{pmatrix}^T \quad (\text{A2})$$

which is used to convert the position errors in the reference Cartesian frame into those in the RTN frame.

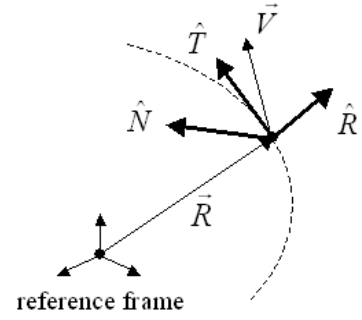


Fig. 8 RTN frame

### Appendix B: UKF Algorithm

Given discrete-time nonlinear state and observation equations

$$X_{k+1} = F(X_k, u_k) + w_k \quad (\text{B1})$$

$$Y_k = G(X_k) + \varepsilon_k \quad (\text{B2})$$

where  $u_k$  is a known input,  $w_k \sim N(0, Q)$  and

$\varepsilon_k \sim N(0, R)$ , the UKF algorithm can be written in the following pseudo-code form<sup>13</sup>.

Initialize with

$$\hat{X}_0 = E[X_0] \quad (\text{B3})$$

$$\hat{P}_0 = E[(X_0 - \hat{X}_0)(X_0 - \hat{X}_0)^T] \quad (\text{B4})$$

For  $k \in \{1, \dots, \infty\}$ ,

$$\mathfrak{S}_{k-1} = \begin{bmatrix} \hat{X}_{k-1} & \hat{X}_{k-1} + \gamma \sqrt{\hat{P}_{k-1}} & \hat{X}_{k-1} - \gamma \sqrt{\hat{P}_{k-1}} \end{bmatrix} \quad (\text{B5})$$

Time update:

$$\mathfrak{S}_{k/k-1} = F[\mathfrak{S}_{k-1}, u_{k-1}] \quad (\text{B6})$$

$$\bar{X}_k = \sum_{i=0}^{2L} W_i^{(m)} \mathfrak{S}_{i,k/k-1} \quad (\text{B7})$$

$$\bar{P}_k = \sum_{i=0}^{2L} W_i^{(c)} [\mathfrak{S}_{i,k/k-1} - \bar{X}_k][\mathfrak{S}_{i,k/k-1} - \bar{X}_k]^T + Q \quad (\text{B8})$$

$$Y_{k/k-1} = G[\mathfrak{S}_{k/k-1}] \quad (\text{B9})$$

$$\bar{Y}_k = \sum_{i=0}^{2L} W_i^{(m)} Y_{i,k/k-1} \quad (\text{B10})$$

Measurement update:

$$\bar{P}_{\tilde{y}_k \tilde{y}_k} = \sum_{i=0}^{2L} W_i^{(c)} [Y_{i,k/k-1} - \bar{Y}_k][Y_{i,k/k-1} - \bar{Y}_k]^T + R \quad (\text{B11})$$

$$\bar{P}_{\tilde{x}_k \tilde{y}_k} = \sum_{i=0}^{2L} W_i^{(c)} [X_{i,k/k-1} - \bar{X}_k][Y_{i,k/k-1} - \bar{Y}_k]^T \quad (\text{B12})$$

$$K_k = \bar{P}_{\tilde{x}_k \tilde{y}_k} \bar{P}_{\tilde{y}_k \tilde{y}_k}^{-1} \quad (\text{B13})$$

$$\hat{X}_k = \bar{X}_k + K_k (Y_k - \bar{Y}_k) \quad (\text{B14})$$

$$\hat{P}_k = \bar{P}_k - K_k \bar{P}_{\tilde{y}_k \tilde{y}_k} K_k^T \quad (\text{B15})$$

where  $\gamma = \sqrt{L + \lambda}$ ,  $\lambda = \alpha^2(L + \kappa) - L$  is a scaling

parameter,  $L$  = dimension of the state,  $Q$  = process noise

covariance,  $R$  = measurement noise covariance, and

$W_i$  = weights given by

$$\begin{aligned} W_0^{(m)} &= \lambda / (L + \lambda) \\ W_0^{(c)} &= \lambda / (L + \lambda) + (1 - \alpha^2 + \beta) \\ W_i^{(m)} &= W_i^{(c)} = 1 / \{2(L + \lambda)\}, i = 1, \dots, 2L \end{aligned} \quad (\text{B16})$$

The constants  $\{\alpha, \beta, \kappa\}$  are adjustable scaling parameters

and their values are usually set in the following way:

$10^{-4} \leq \alpha \leq 1$ ,  $\kappa = 0$  or  $3 - L$ , and  $\beta = 2$  (optimal for Gaussian distributions).

### Takahiro YOSHIOKA



Received the B.E. degree from the Tohoku University in 2005, and the M.E. degree from NDA in 2010. He has been with the Japan Grand Self-Defense Force since March 2005. His field of interest is applied estimation and GPS navigation.

### Masaaki MURATA (Member)



Received the B.E. and M.E. degrees from Kyoto University in 1967 and 1969, respectively, and the Ph.D. degree in aero-space engineering from the University of Texas at Austin in 1982. In 1969, he joined the National Aerospace Laboratory (now JAXA) and worked on satellite geodesy and GPS applications. From April 2003 to March 2010, he was Professor of Aerospace Engineering at the National Defense Academy (NDA). Currently, he is Technical Adviser at GNSS Technologies, Inc. He is a member of the Geodetic Society of Japan and the American Astronautical Society.